chemosensors

MDPI

Article

Ba-Modified ZnO Nanorods Loaded with Palladium for Highly Sensitive and Rapid Detection of Methane at Low Temperatures

Yijing Cai [1,†], Shirui Luo [2,†], Renjie Chen [2], Junxia Yu [1,*] and Lan Xiang [2,*]

[1] Hubei Novel Reactor & Green Chemical Technology Key Laboratory, Key Laboratory for Green Chemical Process of Ministry of Education, School of Chemistry and Environmental Engineering, Wuhan Institute of Technology, Wuhan 430205, China
[2] Department of Chemical Engineering, Tsinghua University, Beijing 100084, China
* Correspondence: 08090201@wit.edu.cn (J.Y.); xianglan@mail.tsinghua.edu.cn (L.X.)
† These authors contributed equally to this work.

Abstract: Exploring novel sensing materials to rapidly identify CH_4 at low temperatures is crucial for various practical applications. Herein, a novel ZnO-xBa/Pd with Ba of cocatalyst loading from 0 to 2.0 wt% was facilely prepared using a two-step impregnation method to improve the sensitivity of the CH_4 gas sensor. The microstructure, chemical states of the elements, and surface properties of ZnO-Ba/Pd were characterized, and the gas-sensitive performance of ZnO-Ba/Pd sensors was investigated. Compared to methane sensors based on other inorganic and organic material sensors, the sensor based on ZnO-1.0Ba/Pd exhibited a faster response/recovery time (1.4 s/8.3 s) and higher response (368.2%) for 5000 ppm CH_4 at a lower temperature (170 °C). Moreover, the ZnO-1.0Ba/Pd sensor exhibited full reversibility and long-term stability, as well as excellent selectivity at 170 °C. The excellent performance of the ZnO-Ba/Pd sensor was attributed to the electron donation by Ba, which increases the electron density around Pd, thus enhancing the catalytic activity of Pd and promoting oxygen adsorption on the ZnO surface. The present work provides a method for the rational design and synthesis of sensitive materials in practical CH_4 detection.

Keywords: methane sensor; ZnO; Pd; Ba; catalytic activity

Citation: Cai, Y.; Luo, S.; Chen, R.; Yu, J.; Xiang, L. Ba-Modified ZnO Nanorods Loaded with Palladium for Highly Sensitive and Rapid Detection of Methane at Low Temperatures. *Chemosensors* **2022**, *10*, 346. https://doi.org/10.3390/chemosensors10090346

Academic Editor: Dario Zappa

Received: 23 July 2022
Accepted: 20 August 2022
Published: 23 August 2022

1. Introduction

Human activities are closely related to methane (CH_4), which is the main component of coal-bed methane and natural gas, and is widely used in industrial production, households, and other fields [1]. However, CH_4 is flammable and highly volatile, with an explosion limit of 5–15% [2]. Therefore, it is critical to design sensors to detect CH_4 gas. In the past few decades, many studies have reported on the development of CH_4 gas sensors based on inorganic and organic materials [3,4]. Jiao et al. employed a rigid tungsten-capped calix [4] arene-based p-doped conducting polymer with PF_6^- or ClO_4^- counter-anions as a transducer in methane detection to achieve experimental and theoretical limits of methane detection (LoD) of <50 and 2 ppm at room temperature, respectively [5]. Zhang et al. integrated a coaxial yarn-shaped G@PVA@GST photoelectrochemical methane sensor in the design and construction, which displayed a rapid response time (0.3 s) and a low detection limit (0.02%) with a linear range of 0.05–0.47% while maintaining favorable selectivity, exceptional bending stability, and sensing reproducibility [6]. Xia et al. presented a novel visible-light photocatalysis-enhanced sensor based on Pd nanoparticle-decorated ZnO/rGO hybrids, enabling high-performance detection of CH_4 at room temperature under visible-light illumination [7]. Among them, metal oxide semiconductor sensors (MOSs) are an excellent choice due to their low cost, high response performance, and simple operation [1,8–11]. Among various MOSs, zinc oxide (ZnO) is widely used, owing to its simplicity of preparation, high electron mobility, and chemical

stability [12–14]. However, pure ZnO suffers from the disadvantages of high operating temperature (>200 °C), low sensitivity, and slow response/recovery, which hinder its further development in practical applications [15].

To further enhance the gas-sensitive performance of ZnO, various strategies, including noble metal doping, defect engineering, and p-n heterostructure construction, have been employed, where noble metal (Au, Ag, Pd, Pt, etc.) doping is the most effective [16–22]. Noble metal doping not only promotes the adsorption and desorption processes of oxygen molecules, but also changes the electronic structure of the metal oxide surface, thus enhancing the gas-sensitive response [8,23]. Among them, ZnO/Pd is an important sensing-system combination. In ZnO-based sensors, Pd is a good catalyst for gas sensing and can effectively improve the sensing performance due to the "spillover effect" [24,25]. Wang et al. reported a response of 19.20 for 5000 ppm CH_4 at 200 °C using Pd as a sensitizer on ZnO nanosheets, which is 2.13 times higher than that of pure ZnO [12]. Zhang et al. reported that 0.5 %Pd/s-ZnO had the highest sensitivity (6.44) to 500 ppm CH_4 at 200 °C, which is about 3.2 times higher than that of pure s-ZnO [26]. Despite this progress, it is still a challenge to develop novel CH_4 sensors to meet the growing demands (e.g., lower operating temperatures and faster response/recovery rates). Since the principle of CH_4 sensing is the catalytic oxidation of CH_4, which is promoted by Pd, it is facile to consider the structural modification of Pd to further improve the CH_4 sensing performance [27]. In recent years, researchers have proposed an important strategy: the introduction of a second metal component as a promoter to enhance the catalytic oxidation of CH_4 at reasonably low temperatures by increasing the activity of the catalyst, which significantly improves the gas sensing performance [28–30]. Among them, using the alkaline earth metal Ba as an electron donor has the advantages of regulating the adsorption/desorption performance of the reaction gas; lowering the gas ignition temperature; stabilizing the active phase; and improving the thermal stability, which could prospectively be introduced as a promoter in Pd-based nanomaterials to achieve fast response/recovery times, high sensitivity, and low operating temperature in CH_4 sensing [31–34].

In this paper, ZnO-xBa/Pd nanorods with Ba content of 0~2.0 wt% were prepared, and the effect of Ba introduction on the CH_4 sensing performance of Pd/ZnO was investigated. Compared to ZnO/Pd sensors, the operating temperature of ZnO-1.0Ba/Pd sensors significantly reduced from 230 °C to 170 °C. The response of ZnO-1.0Ba/Pd to 5000 ppm CH_4 reached up to 368.2%, which is approximately 1.8 times that of ZnO/Pd (205.0%), and the response/recovery times of ZnO-Ba/Pd (1.4/8.3 s) greatly shortened compared to ZnO/Pd (2.7/13.1 s). The introduction of Ba not only enhances the catalytic activity of Pd, but also the increase in adsorbed oxygen promotes the surface oxidation of CH_4, thus enhancing the sensitivity of CH_4. This work provides a novel method for the rapid detection of CH_4 at low temperatures.

2. Materials and Methods

2.1. Synthesis

Based on previous work, ZnO nanorods were synthesized as starting materials using ε-$Zn(OH)_2$ as precursors [15]. In a typical synthesis process of ZnO/Pd, 0.38 g of ZnO nanorods and 0.01 g of $PdCl_2$ were added to 80 mL of ethylene glycol to form a suspension. Then, the suspension was heated at 100 °C for 3 h. Finally, the precipitate was washed and dried overnight at 55 °C to obtain ZnO/Pd. For the synthesis of ZnO-Ba/Pd, a certain amount of $Ba(NO_3)_2$, corresponding to 0, 0.5, 1.0, 1.5, and 2.0 wt% of BaO in the final samples, was firstly dissolved in deionized water to form transparent solutions. Then, 0.38 g of ZnO nanorods was dispersed in the solution, followed by continuous stirring for 1 h. After drying at 60 °C for 12 h and calcining at 250 °C for 1.5 h in air, ZnO-Ba materials were obtained. Subsequently, 0.38 g ZnO-Ba and 0.01 g $PdCl_2$ in 80 mL of ethylene glycol were dispersed to form a suspension. Afterward, the suspension was stirred at 100 °C for 3 h. Finally, the precipitate was washed at 55 °C and dried overnight to obtain ZnO-Ba/Pd.

According to the designed BaO loading, the materials were denoted as ZnO-0.5Ba/Pd, ZnO-1.0Ba/Pd, ZnO-1.5Ba/Pd, and ZnO-2.0Ba/Pd, respectively.

2.2. Characterization

The microstructure and morphology of the samples were examined via field emission scanning electron microscopy (FESEM, JSM 7401F, JEOL, Akishima City, Akishima City, Japan), and high-resolution transmission electron microscopy (HRTEM, JEM-2010, JEOL, Japan), respectively. EDX (Energy Dispersive X-ray Spectroscopy) analysis was performed on several areas for elemental analysis. An inductively coupled plasma (ICP) spectrometer (Thermo IRIS Intrepid II type) was used to detect the actual Ba amount in the samples. A Ba standard solution of 100 ppm was gradiently diluted to establish the calibration curve, and the sample was fully dissolved with 1% dilute sulfuric acid and tested to obtain the accurate concentration of Ba according to the calibration curve. The crystal structure of the samples was analyzed via X-ray powder diffraction (XRD, Bruker D8 Advance), with Cu kα (λ = 0.154178 nm) incidence-radiation. The surface composition of the materials was characterized using X-ray photoelectron spectroscopy (XPS, PHI-5300, PHI, USA). The Software package XPSPeak41 was used for spectral deconvolution. The catalytic decomposition rate of the target gases was determined via gas chromatography (GC, 9790IIT-2, 78 FULI, China) equipped with a flame ionization detector (FID).

2.3. Sensor Fabrication and Response Measurement

The prepared samples were ground in an agate mortar and dispersed in appropriate deionized water to form a homogeneous paste. The paste was then applied to the surface of an alumina ceramic tube with four Pt electrodes on it. The prepared ceramic tubes were dried at 60 °C for 1 h and then calcined at 250 °C for 2 h. A Ni-Cr heating wire was inserted into the tubes to adjust the sensor's operating temperature. The gas sensor was aged at 230 °C for 7 days to improve the stability before sensor testing. Gas sensing tests of the fabricated sensors were performed on the gas sensing analysis system of CGS-8 system (Beijing Elite Tech. Co., Ltd., Beijing, China). The measuring system consists of a data acquisition system, heating system, and test software, and the ambient temperature and relative humidity were 25 °C and 25–30%. The calculated volumes of CH_4 (1000~5000 ppm) gas were injected into a hermetic chamber with a volume of 500 mL using a micro syringe. The response ($\frac{R_a - R_g}{R_g} \times 100\%$) of the sensor is defined as the ratio of the resistance of the sensor in the air (R_a) to the resistance in the target gas (R_g). The time required to reach 90% of the total resistance change is used to estimate the response and recovery time.

2.4. Catalytic Measurements

The catalytic activity of samples was evaluated in a steel microreactor (8.0 mm i.d. × 0.7 m) for the oxidation of CH_4 at ambient pressure. The catalyst (0.4 g) was ground to a 200–300 mesh powder and placed at the center of the microreactor. The CH_4 (37.5 mL min^{-1}) was charged, then mixed with air (75 mL min^{-1} (STD)). The mole ratio was CH_4:O_2:N_2 = 1:1:1. The sample was collected online at 120 °C and quantified by a gas chromatograph (GC, 9790IIT-2, FULI, China) equipped with a flame ionization detector (FID) and a packed column (Porpark N, 3 mm × 5 mm, Hichina Zhicheng Technology Ltd., Shenzhen, China). The methane decomposition ratio was determined by measuring the ratio of input methane to output methane.

3. Results

3.1. Structural and Morphological Characteristics

The construction process of the ZnO-Ba/Pd is schematically illustrated in Figure 1. The material morphology was characterized by SEM and TEM. As seen in Figure 2a, the ZnO-1.0Ba/Pd material presented an urchin-shaped structure that was assembled by uniform nanorods, benefiting the construction of conduction tunnels [15]. According to Figure 2b, Pd nanoparticles with a diameter of 2–5 nm were highly dispersed on the surface of ZnO

nanorods. As shown in Figure 2c, the lattice spacing of 0.224 nm observed in HRTEM images was fitted well with the (111) plane of metallic Pd. The elemental content of the sample was detected by EDX (Figure 2d). Several areas of ZnO-1.0Ba/Pd were examined, and no significant Ba was localized due to the limit of instrumental precision. However, 0.63 wt% of the Ba element was identified by ICP analysis. Therefore, it was concluded that Ba was well dispersed on the ZnO-1.0Ba/Pd, which was further confirmed in the following XPS analysis.

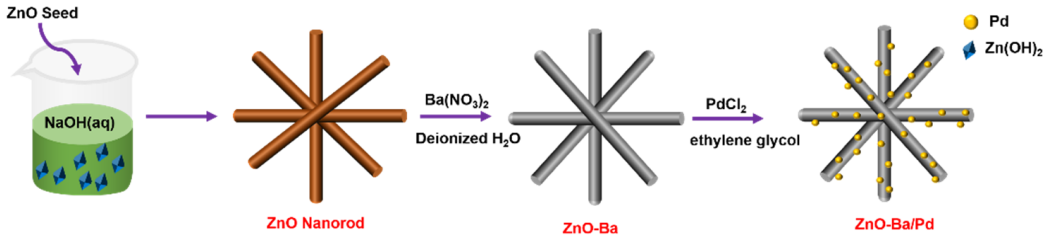

Figure 1. Schematic illustration of the fabrication of ZnO-Ba/Pd sensitive material.

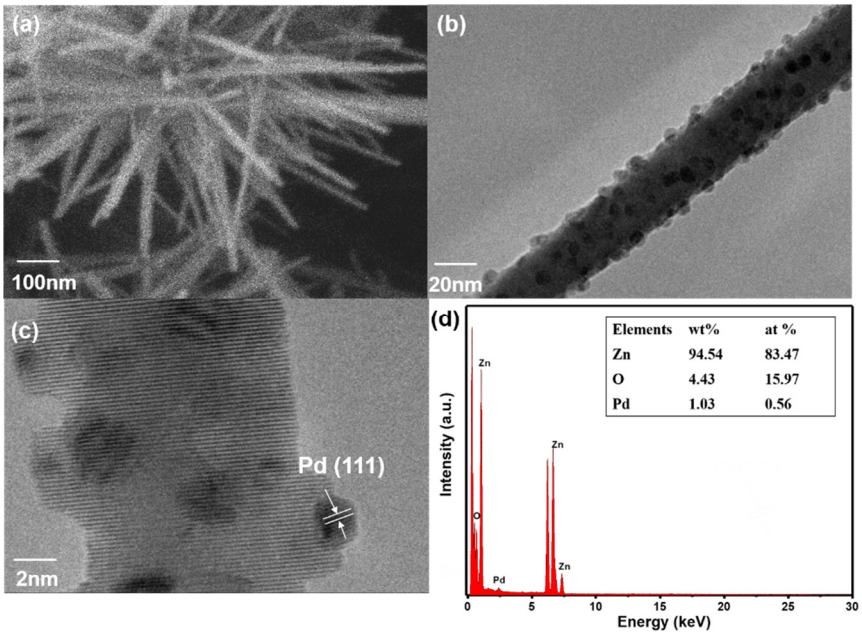

Figure 2. SEM images of (**a**) ZnO-1.0Ba/Pd, (**b**) TEM of ZnO-1.0Ba/Pd, (**c**) HRTEM image of ZnO-1.0Ba/Pd, (**d**) EDX spectrum of ZnO-1.0Ba/Pd.

The crystal structure and phase composition of ZnO-1.0Ba/Pd were characterized via X-ray diffraction (XRD). As shown in Figure 3a, the prepared samples exhibit three major diffraction peaks at 31.8°, 34.5°, and 36.3°, corresponding to the (100), (001), and (101) crystal planes of ZnO (PCPDF 36-1451). The peak situated at 40.2° can be assigned to the (111) crystallographic facet of Pd (PCPDF 89-4897), revealing that Pd NPs were successfully loaded on ZnO. No significant Ba diffraction peaks were observed from the X-ray diffraction patterns of ZnO-1.0Ba/Pd, which may be ascribed to the ultrasmall size and low content of Ba. XPS analysis was used to investigate the chemical state of the elements in the samples. The peaks of Zn, O, Pd, and Ba elements can be seen in a full-range XPS spectrum (Figure 3b). Figure 3c shows two peaks at binding energies of 1021.3 and 1044.4 eV in ZnO-1.0Ba/Pd, corresponding to Zn 2p3/2 and Zn 2p1/2, respectively, with a gap of 23.1 eV in the splitting energy levels, which indicates that Zn exists in the form of Zn^{2+}. The high-resolution O 1s XPS spectra of ZnO/Pd and ZnO-1.0Ba/Pd are displayed in Figure 3d. For the ZnO/Pd sample, three peaks located at 529.8, 530.4, and 531.6 eV can be observed, which correspond to the lattice oxygen (O_{lat}), defect oxygen (O_{def}), and surface-adsorbed oxygen species (O_{ads}), respectively. The O_{ads} component is usually attributed to

chemisorbed and dissociated oxygen species (O_2^-, O^{2-}, or O^-) and other oxygen species (H_2O, OH^-, CO_2, etc.) [35]. The percentages of O_{def} and O_{ads} in pristine ZnO/Pd were 26.4 and 39.7%, respectively, and after the addition of Ba, both increased to 29.5 and 42.23%, respectively. Therefore, ZnO-1.0Ba/Pd provides more adsorbed and defective oxygen than ZnO/Pd, which may facilitate the improvement of gas sensitivity. Figure 3e shows two peaks at binding energies of 780.5 and 795.9 eV, corresponding to Ba^{2+} 3d5/2 and 3d3/2, respectively, with a gap of 15.4 eV in the splitting energy levels. In Figure 3f, the Pd 3d spectrum of ZnO-1.0Ba/Pd presented dominant peaks located at 334.6 and 339.9 eV corresponding to Pd 3d3/2 and Pd 3d5/2, respectively, which were verified as the Pd^0 state [15]. In addition, the deconvolution results show two peaks at 335.5 eV and 341.0 eV, which are attributed to Pd^{2+} 3d5/2 and Pd^{2+} 3d3/2, indicating the presence of PdO on the surface, which may be the result of partial oxidation of Pd nanoparticles [25]. The Pd 3d spectrum of the ZnO/Pd sample can be deconvoluted into four peaks: the peaks of Pd^0 (334.9 and 340.2 eV) and Pd^{2+} (335.6 and 341.1 eV). Compared to ZnO/Pd, the Pd° and Pd^{2+} of ZnO-1.0Ba/Pd were negatively shifted by 0.3 eV and 0.1 eV, respectively, indicating the electron density around Pd in ZnO-1.0Ba/Pd increases as a result of the electron donation from the Ba species.

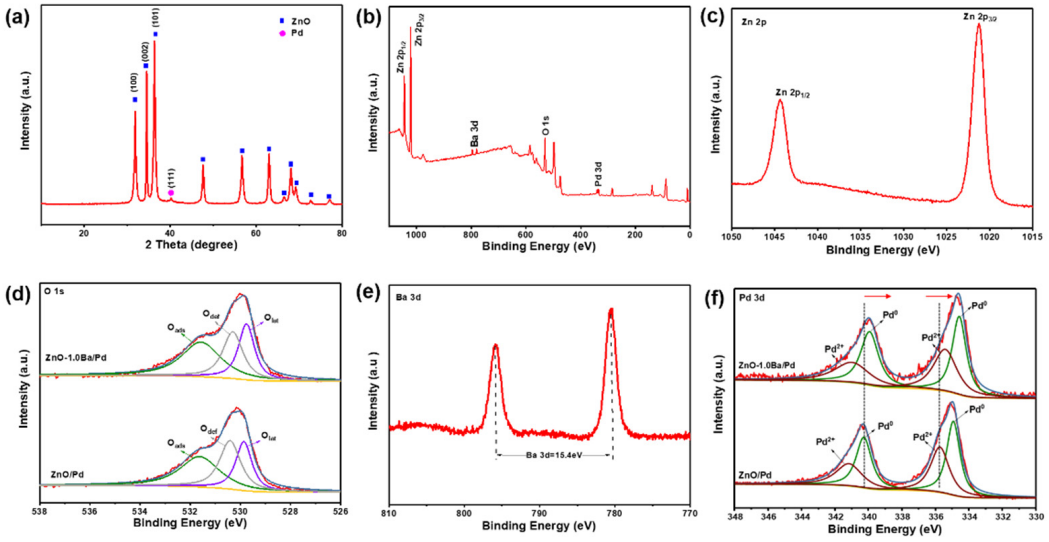

Figure 3. XRD patterns of (**a**) ZnO-1.0Ba/Pd; (**b**) overall XPS spectra of ZnO-1.0Ba/Pd, XPS spectra of ZnO-1.0Ba/Pd; (**c**) Zn 2p spectrum; (**d**) O 1s spectrum; (**e**) Ba 4d spectrum; (**f**) Pd 3d spectrum.

3.2. Gas Sensing Properties

The operating temperature is the primary factor affecting the sensitivity of the material to the target gas. The gas response based on the prepared samples of 5000 ppm CH_4 was examined at the different working temperatures of 120~300 °C to determine the relationship between the gas response and the working temperature. As shown in Figure 4a, a volcano-like correlation between temperature and response was observed. It was found that the optimal operating temperature of pristine ZnO for CH_4 gas is 280 °C, with a maximum response of 32.6%. Significantly, after loading Pd and Ba/Pd, the optimum operating temperature was remarkably reduced and the response increased. The optimal operating temperatures of ZnO/Pd and ZnO-Ba/Pd decreased from 280 °C to 230 °C and 170 °C, respectively. Notably, the optimal operating temperature of ZnO-Ba/Pd plummeted by 110 °C. In addition, the response is affected by the Ba addition, which tends to increase and then decrease in the range of 0.5–2.0 wt%. Among them, the ZnO-1.0Ba/Pd sensor showed maximum sensitivity (368.2%) at 170 °C, which was nearly 1.8 times that of ZnO/Pd (205.0%). This demonstrates the competitive advantage of Ba addition. When a small amount of Ba was added, it was not sufficient to reach full catalytic enhancement (ZnO-0.5Ba/Pd (278.18%)). However, when the Ba addition exceeded 1 wt%, the response

values of ZnO-1.5Ba/Pd and ZnO-2.0Ba/Pd were 288.1 and 219.6%, respectively, and the corresponding response values decreased. Such a phenomenon may be due to the decrease in the active sites of sensitive materials caused by the Ba overloading [28]. These results indicate that only the appropriate amount of Ba loading can effectively improve the sensing performance.

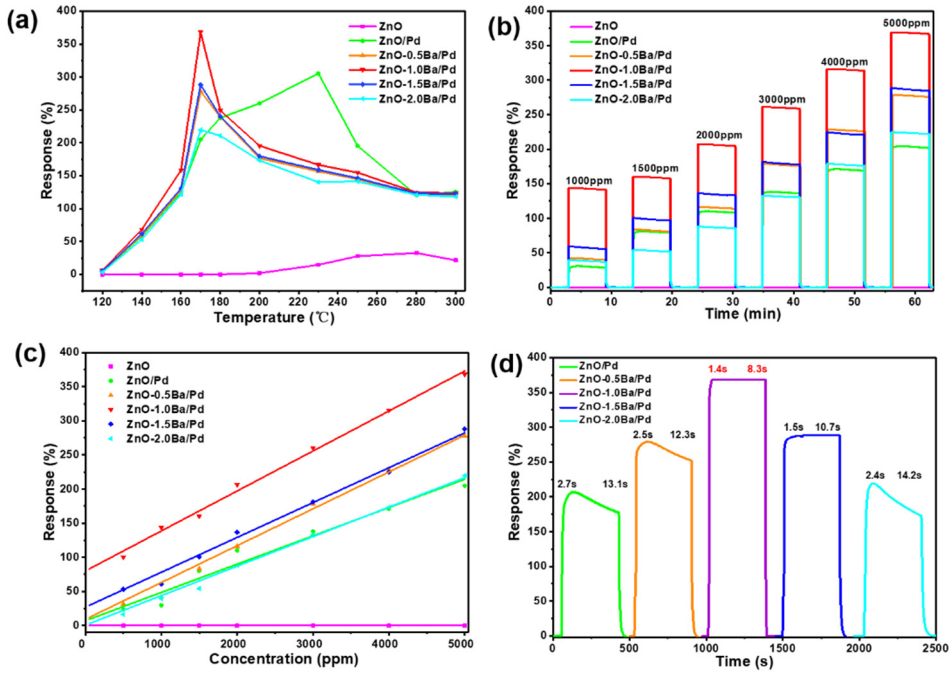

Figure 4. Gas sensing properties of ZnO/Pd, ZnO-0.5Ba/Pd, ZnO-1.0Ba/Pd, ZnO-1.5Ba/Pd, and ZnO-2.0Ba/Pd for 5000 ppm CH_4: (**a**) response at different working temperatures (120–300 °C), (**b**) dynamic response (1000–5000 ppm), (**c**) relationship of the gas response to CH_4 gas concentration (1000–5000 ppm), (**d**) response and recovery curves of sensitive materials.

The time-dependent response of the sensors at 170 °C in the concentration range of 1000–5000 ppm is shown in Figure 4b, indicating excellent reversibility and repeatability. The ZnO-1.0Ba/Pd exhibited a superior CH_4 response (368.2% to 5000 ppm) compared to ZnO/Pd (204.9%), ZnO-0.5Ba/Pd (278.18%), ZnO-1.5Ba/Pd (288.1%), and ZnO-2.0Ba/Pd (219.6%), demonstrating a remarkably improved response due to functionalization of the Ba as a cocatalyst for ZnO/Pd. As shown in Figure 4c, the response values of ZnO-1.0Ba/Pd showed good linearity with wide testing of CH_4 concentrations (1000–5000 ppm), indicating a practical application for quantitative CH_4 detection. For instance, the linear relationship Response= 0.06C+ 88.07 can be fitted to ZnO-1.0Ba/Pd (R^2 = 0.9963), where C is the concentration of the test gas. The response/recovery time is an important parameter in evaluating the practicability of the CH_4 sensor. As shown in Figure 4d, the response/recovery times of the ZnO/Pd, ZnO-0.5Ba/Pd, ZnO-1.0Ba/Pd, ZnO-1.5Ba/Pd, and ZnO-2.0Ba/Pd sensors for 5000 ppm CH_4 were 2.7/13.1 s, 2.5/12.3 s, 1.4/8.3 s, 1.5/10.7 s, and 2.4/14.2 s, respectively. The fast response of the ZnO-1.0Ba/Pd sensor stems from the following factors: first, the unique urchin structure of ZnO provides a large specific surface area, which facilitates the adsorption of gas molecules; second, the catalytic activation of Pd NPs, which is effectively facilitated by Ba, promotes the chemisorption or dissociation kinetics of CH_4, thus accelerating the response/recovery process [36]. When the concentration of the Ba addition was further increased, both reaction/recovery times became longer (1.5/10.7 s and 2.4/14.2 s, respectively), which may be related to the excess Ba loading covering the active site of the material and reducing the reaction rate [37]. Comparing the samples with different Ba concentrations (Figure 5a), the Pd 3d spectrum in ZnO-1.0Ba/Pd showed the highest shift to low-binding energy, indicating the highest electron transfer from Ba to Pd, thus enhancing the catalytic activity of Pd and promoting the catalytic oxidation of

CH_4. The fact that these sensors were exposed to 5000 ppm CH_4 for five consecutive cycles showed that the response–recovery curves were reproducible, with no significant changes (Figure 5b), indicating excellent repeatability. As shown in Figure 5c, the ZnO-1.0Ba/Pd sensor shows a high response of 368.2% to CH_4 (5000 ppm), clearly much higher than other typical gases (54.2% for 24 ppm CO, 42.6% for 24 ppm NH_3, 20.6% for 1 ppm C_7H_8, 25.4% for 1 ppm HCHO, 23.2% for 1 ppm C_6H_6), illustrating excellent selectivity; the maximum allowable concentration of C_7H_8, HCOH, and C_6H_6 is 1 ppm, and the safe concentration of CO, NH_3, and CH_4 in coal mines are 24 ppm, 40 ppm, and 5000 ppm, respectively. Moreover, the long-term stability test for the ZnO/Pd, ZnO-0.5Ba/Pd, ZnO-1.5Ba/Pd, and ZnO-2.0Ba/Pd sensors operated at 170 °C for 30 days at 5000 ppm CH_4 with a 17.5,13.1, and 13.9% decrease, respectively, compared to the original response values (Figure 5d). In contrast, the ZnO-1.0Ba/Pd sensor can maintain its original response with a change of less than 8.5% after 30 days, indicating satisfactory reproducibility and long-term stability. A comparison of the present sensors with other reported CH_4 sensors is summarized in Table 1; the ZnO-1.0Ba/Pd sensor sensing performances are superior to previous CH_4 sensors, indicating that the as-designed sensors are promising for actual CH_4 detection.

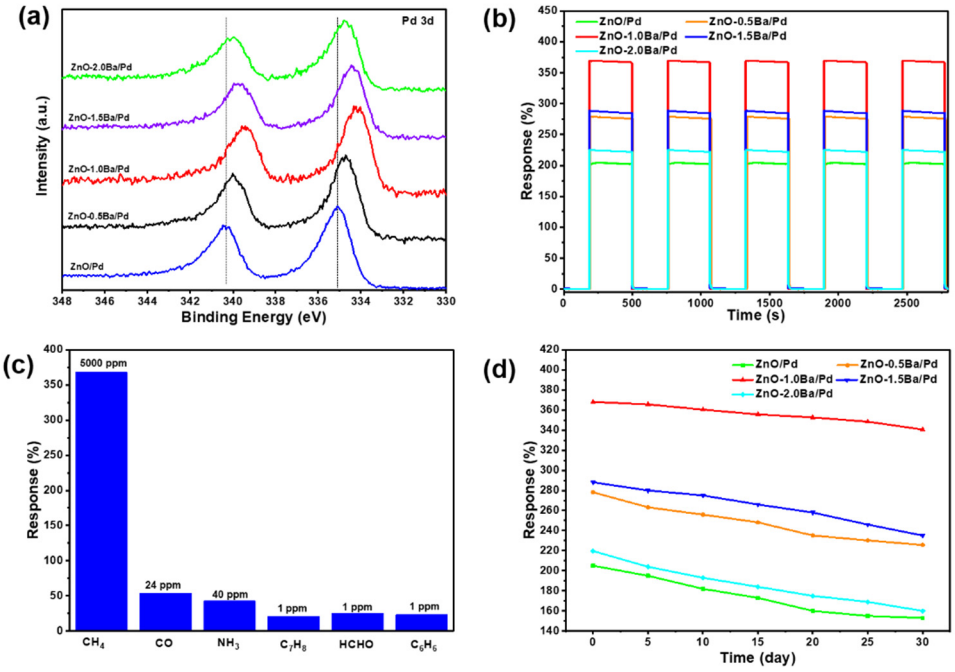

Figure 5. (**a**) The Pd 3d XPS spectra of the different samples; (**b**) reproducibility of ZnO/Pd, ZnO-0.5Ba/Pd, ZnO-1.0Ba/Pd, ZnO-1.5Ba/Pd, and ZnO-2.0Ba/Pd; (**c**) selectivity of ZnO-1.0Ba/Pd at the working temperature of 170 °C; (**d**) stability tests for five ZnO-based sensors.

Table 1. The sensing performance of the CH_4 sensor in this work in comparison to previous reports.

Materials	Tem. (°C)	Con. (ppm)	Res.	Ref.
Pd–Ag/ZnO/Zn	220	10,000	3.81 [a]	[38]
Au/ZnO	250	100	4.16 [a]	[39]
ZnO/rGO	190	1000	12.10% [b]	[40]
Pd–SnO_2	300	250	4.88 [a]	[41]
Pd/ZnO	200	100	8.56 [a]	[12]
NiO/rGO	260	1000	15% [b]	[42]
SnO_2/NiO	330	500	15.2% [b]	[43]
Pd/s-ZnO	190	500	6.44 [a]	[26]
Zn_2SnO_4/ZnO	250	1000	27.2 [a]	[44]
Pt–SnO_2	350	500	21% [b]	[45]
Pt–Ca/SnO_2	400	5000	2.3 [a]	[46]
Ni_2O_3–SnO_2	400	200	127% [a]	[47]
ZnO-1.0Ba/Pd	170	5000	368.2% [b]	This work

Note: The response is defined as: [a] Ra/Rg, [b] (Ra − Rg)/Ra×100%.

3.3. Gas Sensing Mechanism

As an n-type semiconductor material, the ZnO sensors follow a surface resistance-controlled sensing model via the adsorption–reaction–desorption mechanism [8]. When n-type ZnO is exposed to air, oxygen (O_2) molecules are chemisorbed on the surface of ZnO in the form of O_2^- (<100 °C), O^- (100–300 °C), and O^{2-} (>300 °C) by attracting electrons in the conduction band of ZnO [48]. The reactions are as follows:

$$O_2(ads) + e^- \rightarrow O_2^-(ads) \quad (1)$$

$$O^-(ads) + e^- \rightarrow 2O^-(ads) \quad (2)$$

$$O^-(ads) + e^- \rightarrow O^{2-}(ads) \quad (3)$$

Chemisorbed oxygen species thus induce the formation of electron depletion regions on the ZnO surface. Thereafter, when ZnO is exposed to CH_4, the resistivity of ZnO decreases due to the surface reaction between CH_4 and chemisorbed oxygen, generating by-products CO_2 and H_2O [49]. This leads to the back-donation of electrons in the conduction band of ZnO ($R_{air} > R_{gas}$) (Figure 6a). The reaction process is described below:

$$CH_4 + 4O^-_{(ads)} \rightarrow CO_{2(gas)} + 2H_2O_{(gas)} + 4e^- \quad (4)$$

The improved performance of the ZnO-1.0Ba/Pd sensor could be attributed to two aspects. Firstly, introducing the second metal Ba as a promoter helps to improve the catalytic effect of Pd and enhances the sensor performance. The catalytic oxidation properties of CH_4 on ZnO/Pd and ZnO-1.0Ba/Pd samples were examined at 100–300 °C, as shown in Figure 6b. The decomposition efficiency of ZnO-1.0Ba/Pd can reach 55.7% at 170 °C. For ZnO/Pd, only about 25.3% of CH_4 was catalytically oxidized into CO_2 and H_2O, which is much lower than that of ZnO-1.0Ba/Pd. The catalytic activity of the ZnO-1.0Ba/Pd sensor was 2.2 times higher than that of the ZnO/Pd sensor. Therefore, the introduction of Ba promotes the high oxidative catalytic activity of Pd, enabling it to oxidize CH_4 gas more easily and further improving the CH_4 sensing performance. The introduction of Ba to enhance the catalytic activity of Pd is attributed to the strong electron-donating ability of the alkaline earth metal Ba, which can increase the electron density around Pd, improve the catalytic activity of Pd, and promote the catalytic oxidation of CH_4 [28].

In addition, with the introduction of Ba, the surface chemisorbed oxygen component greatly increased (as depicted in Figure 3d), and the increase in the surface chemisorbed oxygen component provided more active sites for the redox reactions occurring on the surface of the sensing material, which induced significant changes in the sensor resistance. As shown in Figure 6c, the baseline resistances of ZnO-1.0Ba/Pd (43.8 MΩ) were significantly higher than those of ZnO/Pd (31.9 MΩ). Once the analyte was introduced, the reaction rate between the chemisorbed oxygen species and CH_4 was enhanced due to the introduction of Ba, which resulted in a larger decrease in resistivity. As shown in Figure 6d, the work functions of BaO, Pd, and ZnO were 1.65, 5.15, and 4.45 eV, respectively [12]. The transfer of electrons from BaO to Pd was consistent with the results obtained from XPS (Figure 3f), improved the catalytic activity of Pd, and promoted the catalytic oxidation of CH_4. The electrons were transferred from ZnO to Pd until the Fermi-level reached equilibrium. Thus, Schottky junctions formed at the interfaces between Pd and ZnO [19]. This process resulted in the extension of the electron depletion layer in the initial state, contributing considerably to the improved CH_4 sensing properties of ZnO-1.0Ba/Pd.

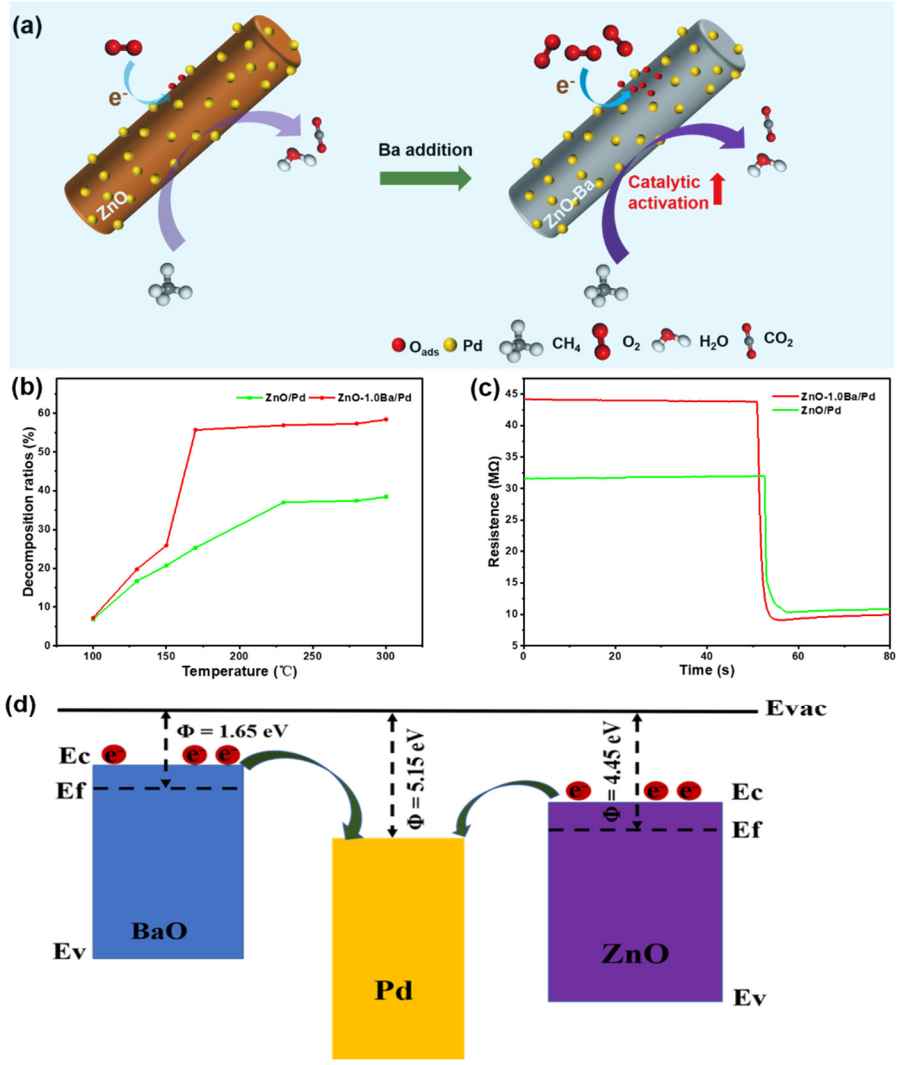

Figure 6. (**a**) Schematic illustration of the CH_4 gas sensing mechanism; (**b**) CH_4 decomposition ratios for ZnO/Pd and ZnO-1.0Ba/Pd at 100–300 °C; (**c**) resistance change curves of sensitive materials before and after target gas injection; (**d**) energy band diagram of BaO, Pd, and ZnO.

4. Conclusions

In summary, Ba-modified ZnO/Pd nanorods were synthesized for efficient CH_4 detection at a low working temperature. The unique urchin structure of ZnO and uniformly dispersed Ba and Pd were characterized by SEM and TEM, and the sensing performance was investigated. The ZnO-1.0Ba/Pd-based sensors exhibited high response performance at 170 °C, with a maximum response value of 368.2% (5000 ppm CH_4) and short response/recovery time (1.4 s/8.3 s), as well as excellent stability. The excellent performance of the ZnO-Ba/Pd sensor is attributed to the electron donation of Ba, which increases the electron density around Pd, thus enhancing the catalytic activity of Pd, and the increase in adsorbed oxygen which also promotes the surface oxidation of CH_4. This study introduces the cocatalytic effect of Ba into the gas sensing mechanism and rationalizes the design of ZnO-Ba/Pd sensors with enhanced CH_4 gas sensing performance, which is expected to provide insights into the synthesis and development of practical CH_4 sensors in the future.

Author Contributions: Conceptualization, methodology, investigation, formal analysis, data curation, visualization, writing original draft, Y.C.; investigation, S.L.; investigation, R.C.; funding acquisition, supervision, J.Y.; resources, supervision, funding acquisition, project administration, L.X. All authors have read and agreed to the published version of the manuscript.

Funding: This research was funded by the National Natural Science Foundation of China, grant number 21978153, the National Key Research and Development Program, grant number 2019YFC1905803, and the Innovative Team program of Natural Science Foundation of Hubei Province, grant number 2021CFA032.

Data Availability Statement: Not applicable.

Conflicts of Interest: The authors declare no conflict of interest.

References

1. Guo, Y.; Liu, C.; Wang, D.; He, R. Advances in the development of methane sensors with gas-sensing materials. *Chin. Sci. Bull.* **2019**, *64*, 1456–1470. [CrossRef]
2. Hong, T.; Culp, J.T.; Kim, K.-J.; Devkota, J.; Sun, C.; Ohodnicki, P.R. State-of-the-art of methane sensing materials: A review and perspectives. *TrAC-Trend Anal. Chem.* **2020**, *125*, 115820. [CrossRef]
3. Qin, T.; Niu, Y.; Qiao, X.; Guo, W.; Zhang, C.; Yang, Z.; Zhang, Y. Integrated coaxial graphene-based yarn with multidimensional architecture for self-powered photoelectrochemical methane sensor. *Sens. Actuators B* **2022**, *365*, 131965. [CrossRef]
4. Dosi, M.; Lau, I.; Zhuang, Y.; Simakov, D.S.A.; Fowler, M.W.; Pope, M.A. Ultrasensitive Electrochemical Methane Sensors Based on Solid Polymer Electrolyte-Infused Laser-Induced Graphene. *ACS Appl. Mater. Interfaces* **2019**, *11*, 6166–6173. [CrossRef]
5. Jiao, M.-Z.; Chen, X.-Y.; Hu, K.-X.; Qian, D.-Y.; Zhao, X.-H.; Ding, E.-J. Recent developments of nanomaterials-based conductive type methane sensors. *Rare Met.* **2021**, *40*, 1515–1527. [CrossRef]
6. Zhang, C.; Guo, W.; Qin, T.; Qiao, X.; Xiao, Z.; Yang, Z. Ultrasensitive self-powered photoelectrochemical detection of methane based on a coaxial integrated carbonene fiber. *Environ. Sci. Nano* **2022**, *9*, 2086–2093. [CrossRef]
7. Xia, Y.; Wang, J.; Xu, L.; Li, X.; Huang, S. A room-temperature methane sensor based on Pd-decorated ZnO/rGO hybrids enhanced by visible light photocatalysis. *Sens. Actuators B* **2020**, *304*, 127334. [CrossRef]
8. Bhati, V.S.; Hojamberdiev, M.; Kumar, M. Enhanced sensing performance of ZnO nanostructures-based gas sensors: A review. *Energy Rep.* **2020**, *6*, 46–62. [CrossRef]
9. Dey, A. Semiconductor metal oxide gas sensors: A review. *Mater. Sci. Eng. B* **2018**, *229*, 206–217. [CrossRef]
10. Debeda, H.; Massok, P.; Lucat, C.; Ménil, F.; Aucouturier, J.L. Methane sensing: From sensitive thick films to a reliable selective device. *Meas. Sci. Technol.* **1997**, *8*, 99. [CrossRef]
11. Lawrence, N.S. Analytical detection methodologies for methane and related hydrocarbons. *Talanta* **2006**, *69*, 385–392. [CrossRef] [PubMed]
12. Wang, Y.; Meng, X.; Yao, M.; Sun, G.; Zhang, Z. Enhanced CH_4 sensing properties of Pd modified ZnO nanosheets. *Ceram. Intc.* **2019**, *45*, 13150–13157. [CrossRef]
13. Yuan, H.; Aljneibi, S.; Yuan, J.; Wang, Y.; Liu, H.; Fang, J.; Tang, C.; Yan, X.; Cai, H.; Gu, Y.; et al. ZnO Nanosheets Abundant in Oxygen Vacancies Derived from Metal-Organic Frameworks for ppb-Level Gas Sensing. *Adv. Mater.* **2019**, *31*, e1807161. [CrossRef] [PubMed]
14. Xia, Y.; Pan, A.; Gardner, D.W.; Zhao, S.; Davey, A.K.; Li, Z.; Zhao, L.; Carraro, C.; Maboudian, R. Well-connected ZnO nanoparticle network fabricated by in-situ annealing of ZIF-8 for enhanced sensitivity in gas sensing application. *Sens. Actuators B* **2021**, *344*, 130180. [CrossRef]
15. Luo, S.; Chen, R.; Wang, J.; Xie, D.; Xiang, L. Designed synthesis of ZnO/Pd@ZIF-8 hybrid structure for highly sensitive and selective detection of methane in the presence of NO_2. *Sens. Actuators B* **2021**, *344*, 130220. [CrossRef]
16. Chen, R.; Wang, J.; Luo, S.; Xiang, L.; Li, W.; Xie, D. Unraveling photoexcited electron transfer pathway of oxygen vacancy-enriched ZnO/Pd hybrid toward visible light-enhanced methane detection at a relatively low temperature. *Appl. Catal. B Environ.* **2020**, *264*, 118554. [CrossRef]
17. Korotcenkov, G.; Cho, B.K. Engineering approaches for the improvement of conductometric gas sensor parameters. *Sens. Actuators B Chem.* **2013**, *188*, 709–728. [CrossRef]
18. Li, C.; Song, B.-Y.; Lv, M.-S.; Chen, G.-L.; Zhang, X.-F.; Deng, Z.-P.; Xu, Y.-M.; Huo, L.-H.; Gao, S. Highly sensitive and selective nitric oxide sensor based on biomorphic ZnO microtubes with dual-defects assistance at low temperature. *Chem. Eng. J.* **2022**, *446*, 136846. [CrossRef]
19. Qin, C.; Wang, B.; Li, P.; Sun, L.; Han, C.; Wu, N.; Wang, Y. Metal-organic framework-derived highly dispersed Pt nanoparticles-functionalized ZnO polyhedrons for ppb-level CO detection. *Sens. Actuators B* **2021**, *331*, 129433. [CrossRef]
20. Hieu, N.M.; Lam, D.V.; Hien, T.T.; Chinh, N.D.; Quang, N.D.; Hung, N.M.; Van Phuoc, C.; Lee, S.-M.; Jeong, J.-R.; Kim, C.; et al. ZnTe-coated ZnO nanorods: Hydrogen sulfide nano-sensor purely controlled by pn junction. *Mater. Des.* **2020**, *191*, 108628. [CrossRef]
21. Lupan, O.; Ababii, N.; Santos-Carballal, D.; Terasa, M.-I.; Magariu, N.; Zappa, D.; Comini, E.; Pauporté, T.; Siebert, L.; Faupel, F.; et al. Tailoring the selectivity of ultralow-power heterojunction gas sensors by noble metal nanoparticle functionalization. *Nano Energy* **2021**, *88*, 106241. [CrossRef]
22. Miller, D.R.; Akbar, S.A.; Morris, P.A. Nanoscale metal oxide-based heterojunctions for gas sensing: A review. *Sens. Actuators B* **2014**, *204*, 250–272. [CrossRef]

23. Wang, Y.; Cui, Y.; Meng, X.; Zhang, Z.; Cao, J. A gas sensor based on Ag-modified ZnO flower-like microspheres: Temperature-modulated dual selectivity to CO and CH_4. *Surf. Interfaces* **2021**, *24*, 101110. [CrossRef]
24. Koo, W.T.; Choi, S.J.; Kim, S.J.; Jang, J.S.; Tuller, H.L.; Kim, I.D. Heterogeneous Sensitization of Metal-Organic Framework Driven Metal@Metal Oxide Complex Catalysts on an Oxide Nanofiber Scaffold Toward Superior Gas Sensors. *J. Am. Chem. Soc.* **2016**, *138*, 13431–13437. [CrossRef] [PubMed]
25. Guo, L.; Wang, Y.; Shang, Y.; Yang, X.; Zhang, S.; Wang, G.; Wang, Y.; Zhang, B.; Zhang, Z. Preparation of Pd/PdO@ZnO-ZnO nanorods by using metal organic framework templated catalysts for selective detection of triethylamine. *Sens. Actuators B* **2022**, *350*, 130840. [CrossRef]
26. Zhang, S.; Li, H.; Zhang, N.; Zhao, X.; Zhang, Z.; Wang, Y. Self-sacrificial templated formation of ZnO with decoration of catalysts for regulating CO and CH_4 sensitive detection. *Sens. Actuators B* **2021**, *330*, 129286. [CrossRef]
27. Chen, Y.; Zhang, W.; Luo, N.; Wang, W.; Xu, J. Defective ZnO Nanoflowers Decorated by Ultra-Fine Pd Clusters for Low-Concentration CH4 Sensing: Controllable Preparation and Sensing Mechanism Analysis. *Coatings* **2022**, *12*, 677. [CrossRef]
28. Du, J.; Guo, M.; Zhang, A.; Zhao, H.; Zhao, D.; Wang, C.; Zheng, T.; Zhao, Y.; Luo, Y. Performance, structure and kinetics of Pd catalyst supported in Ba modified γ-Al2O3 for low temperature wet methane oxidation. *Chem. Eng. J.* **2022**, *430*, 133113. [CrossRef]
29. Klingstedt, F.; Karhu, H.; Neyestanaki, A.K.; Lindfors, L.E.; Salmi, T.; Väyrynen, J. Barium Promoted Palladium Catalysts for the Emission Control of Natural Gas Driven Vehicles and Biofuel Combustion Systems. *J. Catal.* **2002**, *206*, 248–262. [CrossRef]
30. Auvray, X.; Lindholm, A.; Milh, M.; Olsson, L. The addition of alkali and alkaline earth metals to Pd/Al_2O_3 to promote methane combustion. Effect of Pd and Ca loading. *Catal. Today* **2018**, *299*, 212–218. [CrossRef]
31. Friberg, I.; Sadokhina, N.; Olsson, L. Complete methane oxidation over Ba modified Pd/Al_2O_3: The effect of water vapor. *Appl. Catal. B* **2018**, *231*, 242–250. [CrossRef]
32. Xie, J.; Wang, J.; Wang, H.; Li, H.; Wang, J.; Shen, M. Promoted Hydrothermal Stability of Pd/CeO_2 Catalyst by Ba Doping. *Catal. Lett.* **2018**, *148*, 2596–2607. [CrossRef]
33. Modwi, A.; Taha, K.K.; Khezami, L.; Al-Ayed, A.S.; Al-Duaij, O.K.; Khairy, M.; Bououdina, M. Structural and Electrical Characterization of Ba/ZnO Nanoparticles Fabricated by Co-precipitation. *J. Inorg. Organomet. Polym. Mater.* **2019**, *30*, 2633–2644. [CrossRef]
34. Chen, X.; Lin, J.; Zheng, Y.; Zhan, Y.; Zhang, W.; Xiao, Y.; Zheng, Y.; Jiang, L. Catalytic methane oxidation performance over $Pd/\gamma\text{-}Al_2O_3$ catalyst optimized by the synergy of phosphorus and MOx (M = La, Ba and Zr). *Fuel* **2021**, *299*, 120933. [CrossRef]
35. Lu, Y.; Zhan, W.; He, Y.; Wang, Y.; Kong, X.; Kuang, Q.; Xie, Z.; Zheng, L. MOF-templated synthesis of porous Co_3O_4 concave nanocubes with high specific surface area and their gas sensing properties. *ACS Appl. Mater. Interfaces* **2014**, *6*, 4186–4195. [CrossRef] [PubMed]
36. Wang, G.; Meng, M.; Zha, Y.; Ding, T. High-temperature close coupled catalysts $Pd/Ce–Zr–M/Al_2O_3$ (M = Y, Ca or Ba) used for the total oxidation of propane. *Fuel* **2010**, *89*, 2244–2251. [CrossRef]
37. Liotta, L. Thermal stability, structural properties and catalytic activity of Pd catalysts supported on $Al_2O_3–CeO_2–BaO$ mixed oxides prepared by sol–gel method. *J. Mol. Catal. A Chem.* **2003**, *204–205*, 763–770. [CrossRef]
38. Aghagoli, Z.; Ardyanian, M. Synthesis and study of the structure, magnetic, optical and methane gas sensing properties of cobalt doped zinc oxide microstructures. *J. Mater. Sci. Mater. Electron.* **2018**, *29*, 7130–7141. [CrossRef]
39. Zhang, B.; Wang, Y.; Meng, X.; Zhang, Z.; Mu, S. High response methane sensor based on Au-modified hierarchical porous nanosheets-assembled ZnO microspheres. *Mater. Chem. Phys.* **2020**, *250*, 123027. [CrossRef]
40. Basu, P.K.; Bhattacharyya, P.; Saha, N.; Saha, H.; Basu, S. The superior performance of the electrochemically grown ZnO thin films as methane sensor. *Sens. Actuators B Chem.* **2008**, *133*, 357–363. [CrossRef]
41. Yang, L.; Wang, Z.; Zhou, X.; Wu, X.; Han, N.; Chen, Y. Synthesis of Pd-loaded mesoporous SnO_2 hollow spheres for highly sensitive and stable methane gas sensors. *RSC Adv.* **2018**, *8*, 24268–24275. [CrossRef] [PubMed]
42. Zhang, D.; Chang, H.; Li, P.; Liu, R. Characterization of nickel oxide decorated-reduced graphene oxide nanocomposite and its sensing properties toward methane gas detection. *J. Mater. Sci. Mater. Electron.* **2015**, *27*, 3723–3730. [CrossRef]
43. Zhang, S.; Li, Y.; Sun, G.; Zhang, B.; Wang, Y.; Cao, J.; Zhang, Z. Enhanced methane sensing properties of porous NiO nanaosheets by decorating with SnO_2. *Sens. Actuators B* **2019**, *288*, 373–382. [CrossRef]
44. Li, X.; Li, Y.; Sun, G.; Zhang, B.; Wang, Y.; Zhang, Z. Enhanced CH_4 sensitivity of porous nanosheets-assembled ZnO microflower by decoration with Zn_2SnO_4. *Sens. Actuators B* **2020**, *304*, 127374. [CrossRef]
45. Lu, W.; Ding, D.; Xue, Q.; Du, Y.; Xiong, Y.; Zhang, J.; Pan, X.; Xing, W. Great enhancement of CH_4 sensitivity of SnO_2 based nanofibers by heterogeneous sensitization and catalytic effect. *Sens. Actuators B* **2018**, *254*, 393–401. [CrossRef]
46. Min, B.-K.; Choi, S.-D. Undoped and 0.1 wt.% Ca-doped Pt-catalyzed SnO_2 sensors for CH_4 detection. *Sens. Actuators B Chem.* **2005**, *108*, 119–124. [CrossRef]
47. Vuong, N.M.; Hieu, N.M.; Hieu, H.N.; Yi, H.; Kim, D.; Han, Y.-S.; Kim, M. Ni_2O_3-decorated SnO_2 particulate films for methane gas sensors. *Sens. Actuators B* **2014**, *192*, 327–333. [CrossRef]
48. Ramgir, N.S.; Ghosh, M.; Veerender, P.; Datta, N.; Kaur, M.; Aswal, D.K.; Gupta, S.K. Growth and gas sensing characteristics of p- and n-type ZnO nanostructures. *Sens. Actuators B* **2011**, *156*, 875–880. [CrossRef]
49. Yang, B.; Zhang, Z.; Tian, C.; Yuan, W.; Hua, Z.; Fan, S.; Wu, Y.; Tian, X. Selective detection of methane by HZSM-5 zeolite/Pd-SnO_2 gas sensors. *Sens. Actuators B* **2020**, *321*, 128567. [CrossRef]